Effect of Carbon Black Addition and Its Phase Selective Distribution on the Stress Relaxation Behavior of Filled Thermoplastic Vulcanizates

Hai Hong Le, Daniel Heidenreich, Igor S. Kolesov, Sybill Ilisch, Hans-Joachim Radusch

Center of Engineering Sciences, Polymer Technology, Martin Luther University Halle-Wittenberg, Halle D-06099, Germany

Received 12 February 2009; accepted 16 May 2009
DOI 10.1002/app.30769
Published online 27 April 2010 in Wiley InterScience (www.interscience.wiley.com).

ABSTRACT: The long term mechanical behavior of thermoplastic vulcanizates (TPV) based on polypropylene (PP) and ethylene propylene diene terpolymer (EPDM) and different types and concentrations of carbon black (CB) has been characterized by means of stress relaxation experiments. Evaluation of the relaxation curves was carried out using the two-component model allowing a division of the initial stress into different stress components which are caused by different networks available in TPV. The discussion focussed on the background of the stress components, which are originated by the CB addition, the non-relaxing stress components $\sigma_{\infty}^{CB(polymer-layer)}$, and $\sigma_{\infty}^{CB(network)}$, as well as the relaxing stress components $\Delta\sigma^{CB(polymer\text{-}layer)}$ and $\Delta\sigma^{CB(network)}$. It was found that the concentration and type of CB as well as the phase specific CB distribution strongly affect the non-relaxing and relaxing stress components. Up to a CB concentration of 9% in the EPDM phase the composite behaves as a thermo-rheologically simple material because the impact of CB addition on the α-relaxation of the crystalline PP phase is still negligible. A master curve was created by the horizontal shift of the relaxing stress curves $\Delta\sigma^{Comp}(t)$ to a reference curve. At higher local CB loadings the additional relaxation processes induced by CB addition overlap with the α-relaxation, thus, no master curve could be made in that case. © 2010 Wiley Periodicals, Inc. J Appl Polym Sci 117: 2622–2634, 2010

Key words: relaxation; thermoplastic vulcanizates; fillers; networks

INTRODUCTION

Thermoplastic vulcanizates (TPV) are produced by melt mixing of a thermoplastic with a rubber and simultaneously curing of the rubber phase during compounding. The microstructure of TPV consists of a thermoplastic matrix (continuous phase) containing dispersed cured rubber domains.[1–3] A number of commercial TPV has been developed for various applications in automotive parts, cable insulation, footwear, packaging, and medical industries because of their excellent weatherability, low density, and relatively low cost.

The addition of fillers, such as glass fibers, carbon black, talc, and calcium carbonate to the TPV improve properties like stiffness, heat distortion temperature, and dimensional stability. The structure development, rheological behavior, as well as mechanical and electrical properties of carbon black-filled TPV were studied frequently.[4–6] The phase specific CB distribution and the related damping behavior were found to be dependent upon the mixing condition and route of CB feeding. CB filled TPV on the basis of PP and NBR exhibits high electrical conductivity at a low percolation threshold of 4% owing to the localization of CB aggregates at the boundary of the cured NBR domains.[4] Flow behavior of TPV follows the power-law behavior showing typical pseudoplastic characteristics. Higher non-linear and non-terminal melt rheological characteristics of dynamic elastic modulus received at low frequency region indicates the formation of nanoscale conducting multiple networks throughout the continuous TPV matrix. Tensile strength and rupture energy increased with carbon black loading.[6]

Regarding the viscoelastic behavior, TPV are influenced strongly by the thermoplastic nature of the PP matrix. That results in a considerable dependence of the mechanical properties on time and temperature. Thus, for a confident application of these materials a detailed knowledge about their viscoelastic especially long-term performance is required. Although the viscoelastic behavior of the unfilled TPV has been investigated,[7–11] the influence of filler addition and its distribution has not been sufficiently investigated so far. In this work, the two-component model proposed by Seeger,[12,13] Krausz and Erying,[14] and Ferry[15] was

Correspondence to: H.-J. Radusch (hans-joachim.radusch@iw.uni-halle.de).

Contract grant sponsor: German Research Foundation (DFG).

© 2010 Wiley Periodicals, Inc.

TABLE I
Structural Parameters of CBs Investigated

CB type	DBP (ml/100 g)	NSA (m^2/g)
CB1: N 220	120	115
CB2: EC 300	327	800

used to characterize the effect of CB addition on the stress relaxation behavior of TPV by correlating the structural features of TPV compounds and the effect of CB content, type and phase specific distribution on it.

MATERIALS AND COMPOSITE PREPARATION

Materials

The semi-crystalline ethylene propylene diene terpolymer (EPDM) Nordel IP 4760P (Dow Chemicals, Germany) with a Mooney viscosity (1 + 4) at 125°C of 60 mL, an ethylene content of 67%, an ENB content of 4.9% and a molecular weight M_W of 170,000 g/mol was used as rubber component. The semi-crystalline polypropylene (iPP) Stamylan P 14 (Sabic Euro Petrochemicals, Gelsenkirchen, Germany) was used as thermoplastic component. Phenolic resin Vulkaresen PA 510 (Vianova Resins, Wiesbaden, Germany) acted as cross-linking agent. Two types of CB were used as fillers, N 220 (Evonik) und EC 300 (Akzo Nobel Chemicals, Germany). They differ considerably from each other through their specific surface area. The structural parameters of both CB are given in Table I.

Mixing regime and sample preparation

TPV were prepared using a double-rotor lab mixer PolyLab System Rheocord (Thermo Electron/Haake, Karlsruhe, Germany) with a rotor speed of 65 rpm and a starting temperature of 180°C. The composition and mixing regime of the unfilled TPV is given in Table II.

The CB concentrations of 9% and 16% with respect to the mass of the composites were chosen (Table III). To localize CB selectively in the EPDM phase (series E) or PP phase (series P), CB was added into the mixing chamber before or after the dynamic vulcanization, respectively, according to the mixing regime given in Tables IV and V. A weight ratio of EPDM to PP was kept constant at 65/35 for all composites.

TABLE II
Composition and Mixing Regime of TPV

Mixing time, (min)	Ingredients	Weight fraction, (part)
0	EPDM	65
2	PP	35
6	Cross-linking agent	3.25
14	Stopped and dumped	

The local concentration of CB with respect to the weight fraction of the EPDM and PP phase, respectively, can be calculated from the total CB concentration and the EPDM/PP ratio. In Table VI, the local CB concentration of all composites is displayed.

For the investigation of formation of the CB network in the blend phases, CB filled EPDM and PP, respectively, with CB concentrations given in Table VI were prepared. Those compounds represent the corresponding phase of the composites.

After discharge from the mixer, all samples were compression-molded at a temperature of 200°C and a pressure of 70 bar for 5 min to get sheets of 1 mm thickness for producing specimens for the stress relaxation experiments.

Morphology characterization, thermal and mechanical testing

Optical microscopy

Optical microscopy has been used to characterize the macrodispersion of CB. We produced gloss cuts by cutting stretched samples by a razor blade at room temperature and analyzed the cut surface by optical microscopy. If the surface of the cut contents CB agglomerates or aggregates, the light scatters at this place and its area appears dark. With an image analysis program one can calculate the area of visible CB regions. The degree of the macrodispersion was assessed as the amount of the non-dispersed agglomerates with an average diameter larger than 6 μm according to eq. (1). A dispersion index of 100% means, that no agglomerate size larger than 6 μm could be found in the cut surface. From every

TABLE III
Composition of the Investigated Composites

	Sample	TPV (%)	CB 1 (%)	CB 2 (%)	CB addition
	TPV	100			No
Series E	C-9CB1-E	91	9		
	C-16CB1-E	84	16		Before dynamic vulcanization
	C-9CB2-E	91		9	
Series P	C-9CB1-P	91	9		
	C-16CB1-P	84	16		After dynamic vulcanization
	C-9CB2-P	91		9	

TABLE IV
Mixing Regime of Composites C-9CB1-E, C-16CB1-E, and C-9CB2-E

Mixing time (min)	Ingredients
0	EPDM
2	CB 1 or CB 2
10	PP
14	Cross-linking agent
20	Stopped and dumped

sample six pictures were made and from every picture six images were analyzed.

$$D = 100\% - A/A_0 \quad (1)$$

A is the sum of all areas of agglomerates with a diameter larger than 6 μm, A_0 is the area of the investigated image.

Atomic force microscopy (AFM)

The phase morphology was investigated using an atomic force microscope (AFM) (Q-Scope 250) (Quesant, Santa Cruz, CA) under intermittendent mode. The cantilever stiffness is $40N/m$ and the resonance frequency nearly 170 kHz. Samples were cryo-cut by means of a microtome HM 360/CM 30 (Microm, Walldorf, Germany) at −110°C with a diamond knife in order to get a smooth surface of the sample.

Electrical volume resistivity measurement

Electrical volume resistivity measurements for low conductive samples were performed at room temperature using an electrometer 6517 A (Keithley) and a measuring cell 8009 resistivity test fixture (Keithley). For high conductive samples a multimeter 2750 (Keithley) was used.

Differential scanning calorimetry

A heat flux calorimeter differential scanning calorimetry (DSC) 820 (Mettler Toledo) equipped with a liquid nitrogen cooling assembly was used to investigate the thermal behavior of the samples. Temperature range selected was from −80°C to 180°C with a heating and cooling rate of 10 K/min. The degree of crystallinity X_C^{EPDM} and X_C^{PP} of the EPDM and PP phase, respectively, was calculated according to eqs. (2) and (3).

$$X_C^{EPDM} = \frac{1}{\varphi_{EPDM}} \frac{\Delta H_f^{EPDM}}{\Delta H_f^{0(PE)}} \quad (2)$$

$$X_C^{PP} = \frac{1}{\varphi_{PP}} \frac{\Delta H_f^{PP}}{\Delta H_f^{0(PP)}} \quad (3)$$

where φ_{PP} and φ_{EPDM} are the weight fractions of the PP and EPDM in composites. ΔH_f^{EPDM} and ΔH_f^{PP} are the melting enthalpy calculated from the area under the melting peak. $\Delta H_f^{0(PE)}$ and $\Delta H_f^{0(PP)}$ are the melting enthalpy of the entirely crystalline substance ($\Delta H_f^{0(PE)} = 293$ J/g,[16] $\Delta H_f^{0(PP)} = 209$ J/g[17]).

TABLE V
Mixing regime of composites C-9CB1-P, C-16CB1-P, and C-9CB2-P

Mixing time min	Ingredients
0	PP
1	EPDM
4	Cross-linking agent
8	CB 1 or CB 2
20	Stopped and dumped

TABLE VI
Local Concentration of CB in the EPDM and PP Phase

	Local CB concentration	
Composite	EPDM phase (%)	PP phase (%)
C-9CB1-E	15	
C-9CB2-E	15	
C-16CB1-E	29	
C-9CB1-P		28
C-9CB2-P		28
C-16CB1-P		54

Dynamic mechanical analysis (DMA)

Dynamic mechanical behavior was characterized using a dynamic mechanical analyzer DMTA Mark 3E (Rheometric Scientific) in tensile mode at a frequency of 1 Hz at different temperatures ($-135°C < T < 170°C$) with a heating rate of 2 K/min.

Stress relaxation experiment

Stress relaxation experiments were performed using a universal testing machine 1425 (Zwick, Roell) in tensile mode. The instrument was equipped with a temperature chamber enabling a long-term constancy of the temperature (deviation < 0.1 K). Dumbbell-shaped specimens were used with an initial length of 20 mm; the clamp distance was 50 mm. A crosshead speed of 50 mm/min was applied. Relaxation curves for all the samples were recorded at a draw ratio $\lambda = 2.0$ (100% deformation) within the temperature range from 30°C to 120°C over a period of 3 to 15 h depending on test temperatures. No steady state stress value was observed even after 15 h. Therefore, an extrapolation method proposed by Li[18] was used to determine the non-relaxing stress component σ_∞.

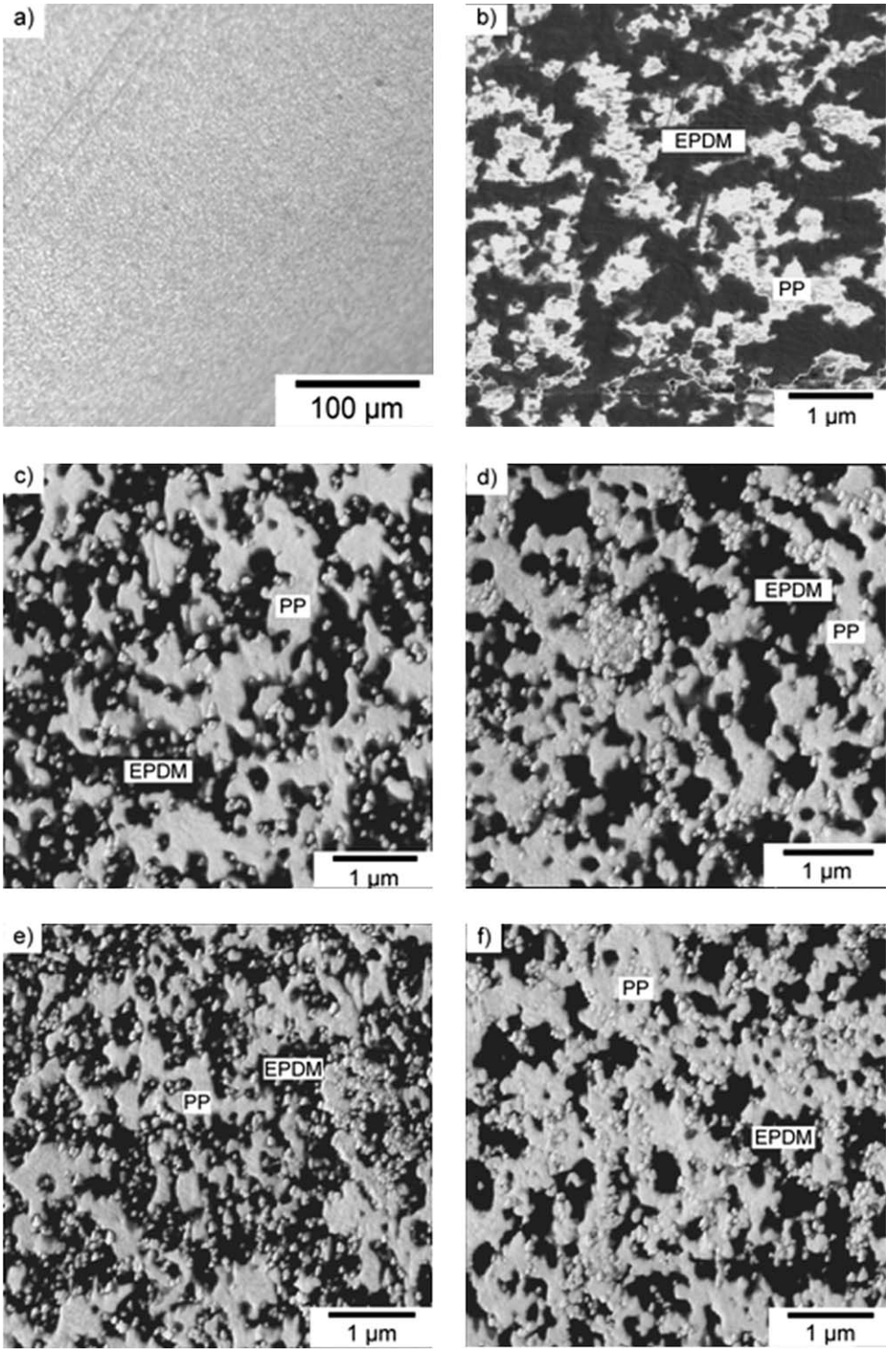

Figure 1 Image of C-9CB1-E made by optical microscopy (a), AFM images of TPV (b), C-9CB1-E (c), C-9CB1-P (d), C-9CB2-E (e), and C-9CB2-P (f).

RESULTS AND DISCUSSION

Structural investigation

The macrodispersion *D* of all composites was investigated by means of optical microscopy. It was found to be nearly 100%. As an example an image of C-9CB1-E is shown in Figure 1(a). No CB aggregate is observed in this image.

AFM images of TPV and composites are depicted in Figure 1(b–f). The unfilled TPV shows a typical island-matrix structure with cross-linked EPDM domains finely distributed in the PP matrix [Fig.

TABLE VII
Electrical Volume Resistivity of CB-Filled EPDM and PP Compounds

Sample	Corresponding composite	Electrical volume resistivity (Ωcm)	Network formation
EPDM + 15% CB1	C-9CB1-E	4.05×10^{14}	non
EPDM + 15% CB2	C-9CB2-E	8.58×10^{3}	moderate
EPDM + 29% CB1	C-16CB1-E	1.91×10^{5}	moderate
PP + 28% CB1	C-9CB1-P	1.46	strong
PP + 28% CB2	C-9CB2-P	0.44	strong
P + 54% CB1	C-16CB1-P	0.27	strong

1(b)]. When CB was first mixed with EPDM before the dynamic vulcanization process according to Table IV, CB is localized mainly in the EPDM domains as seen in Figure 1(c,e). If CB was added into the mixture after the dynamic vulcanization processes then CB is distributed mainly in the PP phase. CB aggregates can not entry the cross-linked EPDM domains as observed in Figure 1(d,f). CB1 shows larger aggregates than CB2 by comparison Figure 1(c,d) with Figure 1(e,f). It is obvious that CB1 and CB2 form a throughout network in the PP phase [Fig. 1(d,f)]. In C-9CB1-E, CB1 exists as separate aggregates in the EPDM phase. In C-9CB2-E, CB2 aggregates become much smaller and they tend to form a network in the EPDM phase.

To get better insight into the formation of CB network the electrical resistivity of CB filled EPDM and PP compounds was investigated and presented in Table VII. In C-9CB1-E, CB1 can not form any network that causes a high volume resistivity of 4.05×10^{14} Ωcm. For C-9CB2-E and C-16CB1-E values of 8.58×10^{3} and 1.9×10^{5} Ωcm were received indicating formation of a moderate CB network. In series P, all composites show very low resistivity that indicates a very strong CB network as observed in Figure 1(d,f). The CB concentration in the present work is in the same order with the concentration reported by Koszkul.[19] He found a percolation threshold of 10% and 20% for PP filled with two types of CB.

TABLE VIII
Crystallization Temperatures T_C^{EPDM}, T_C^{PP} and Degree of Crystallinity X_C^{EPDM}, X_C^{PP} of Two Phases of TPV and the Investigated Composites

Sample	T_C^{EPDM}	X_C^{EPDM} (%)	T_C^{PP}	X_C^{PP} (%)
TPV	21	8.43	121	38.85
C-9CB1-E	21	8.4	121	39.3
C-9CB2-E	21	8.32	121	38.48
C-16CB1-E	21	7.26	120	40.08
C-9CB1-P	21	8.78	120	40.17
C-9CB2-P	21	9.01	119	41.05
C-16CB1-E	21	8.93	119	39.12

DSC thermograms of TPV and both composites C-9CB1-E and C-9CB1-P are presented in Figure 2. A broad peak between −50°C and 60°C is formed by two processes: the cooperative segmental relaxation process of the amorphous EPDM phase (glass transition) taking place in the temperature range between −50°C and −20°C, and the melting process of the crystalline EPDM phase formed by ethylene segments starting at around −20°C and ending at $T_{m,\text{end}}^{\text{EPDM}} = 60$°C. At $T_{m,\text{onset}}^{\text{PP}} = 105$°C the crystalline PP phase starts to melt. The melting temperature $T_m^{\text{PP}} = 160$°C is determined as the position of the peak maximum. Addition of CB into the EPDM and PP phase, respectively, alters the crystallinity of both phases only insignificantly as seen in Table VIII.

The temperature dependence of the loss factor tan δ of the unfilled TPV and composites C-9CB1-E and C-9CB1-P is presented in Figure 3. The neat TPV shows the characteristic glass transition of the amorphous EPDM phase at temperatures ranging from

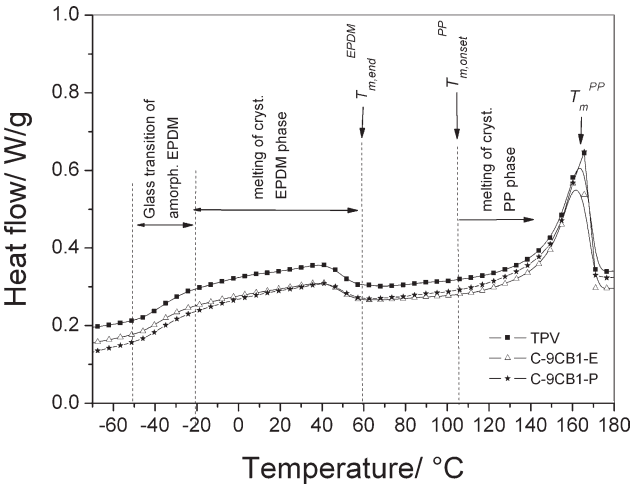

Figure 2 DSC thermograms of TPV and the composites C-9CB1-E and C-9CB1-P.

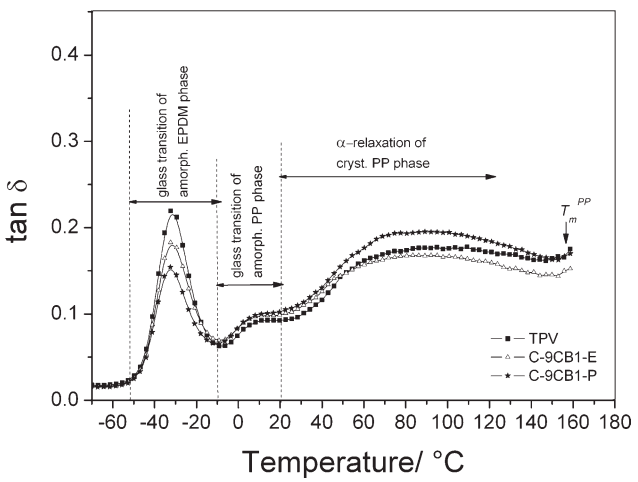

Figure 3 Loss factor tan δ of the TPV and the composites C-9CB1-E and C-9CB1-P.

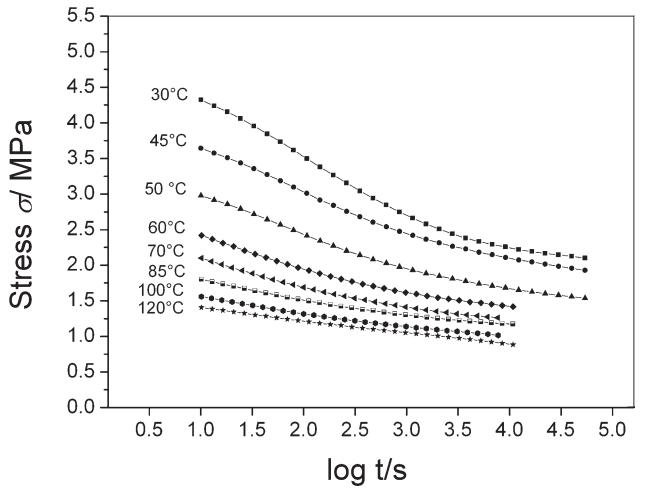

Figure 4 Stress relaxation of TPV in dependence on the test temperatures.

−50°C to −10°C. A small peak appears between −10°C and 20°C is identified as the β-relaxation process (glass transition) of the amorphous PP phase. It is followed by a broad peak ranging from 30°C to $T_m^{PP} = 160$°C which is caused by the α-relaxation processes of the crystalline PP phase.

Relaxation behavior of unfilled TPV

To evaluate the relaxation curve, among different models the two-component model has been frequently used. On the basis of it the relaxation curve $\sigma(t)$ can be separated into two components, a relaxing curve $\Delta\sigma(t)$ and a non-relaxing stress component σ_∞[12–15]:

$$\sigma(t) = \Delta\sigma(t) + \sigma_\infty \quad (4)$$

When $t \to \infty$ the initial stress value σ is the sum of the relaxing stress component $\Delta\sigma$ and the non-relaxing stress one σ_∞:

$$\sigma = \Delta\sigma + \sigma_\infty \quad (5)$$

According to Seeger[12,13] the relaxing stress component $\Delta\sigma$ is called thermally activated stress component, because it acts on short-range obstacles, which can be overcome by stress aided thermal activation. It depends on the plastic deformation rate and temperature according to Eyring's rate theory.[14] In contrast to the relaxing stress component $\Delta\sigma$, the non-relaxing stress component σ_∞ is called athermal stress component. It is originated from long-range stress fields, which can not be overcome by thermal activation.On the basis of the two-component model we have developed an evaluation method for characterization of the stress relaxation behavior of the multi-component polymer systems.[7] The basis idea is to consider the investigated system as a combination of different networks. A systematic variation of material parameters and test conditions allows us to separate the initial stress σ into different components and to attribute them to the according networks in the system. The proposed method was successfully applied for evaluation of the time and temperature dependent deformation behavior of the unfilled thermoplastic elastomers TPE[7] and the oil extended TPE[8] as well.

Figure 4 shows the stress relaxation curves of unfilled TPV measured at different temperatures. With increasing temperature the relaxation curves shift horizontally to shorter times and vertically to lower stress. The horizontal shift is caused by a reduction of the thermal stress component $\Delta\sigma$ and the vertical shift is originated from a linear decrease of the athermal stress component σ_∞.[20]

According to the eq. (5) the initial stress σ^{TPV} of TPV is divided into the relaxing stress component $\Delta\sigma^{TPV}$ and the non-relaxing stress component σ_∞^{TPV}. Based on the previous works,[7,8,20] the non-relaxing stress σ_∞^{TPV} consists of three components: the stress contributions of the crystalline EPDM phase $\sigma_\infty^{TPV(crystEPDM)}$ and the crystalline PP phase $\sigma_\infty^{TPV(crystPP)}$ as well as the stress contribution of the chemically cross-linked EPDM phase $\sigma_\infty^{TPV(chemEPDM)}$. They are clearly identified in Figure 5 by extrapolating $\sigma_\infty^{TPV(crystPP)}$ and $\sigma_\infty^{TPV(chemEPDM)}$ to lower temperature range. The decrease of σ_∞^{TPV} with temperature is explained as a result of the temperature dependent change of the crystalline network in EPDM and PP phase which can be described by straight lines.

In the EPDM phase, a crystalline network is created by the crystallites of ethylene segments, which melts when temperature increases up to $T_{m,end}^{EPDM} = 60$°C. At this temperature the contribution of the crystalline network of the EPDM phase $\sigma_\infty^{TPV(crystEPDM)}$ disappears

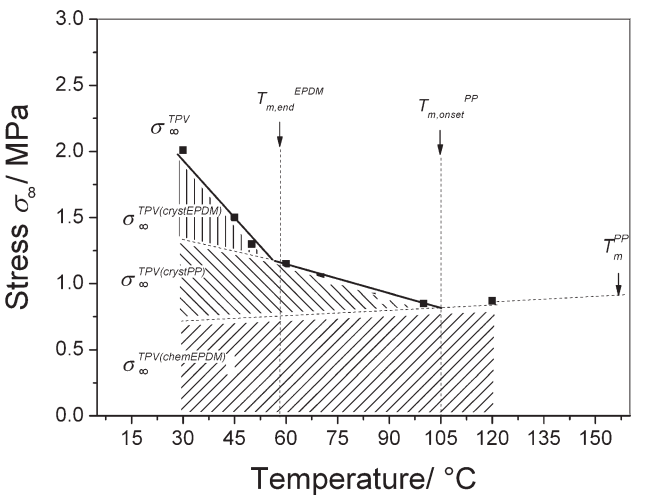

Figure 5 Non-relaxing stress σ_∞^{TPV} of TPV in dependence on the test temperatures.

TABLE IX
Molecular Weight Between Two Net Points of Different Networks

Temp [°C]	30	45	50	70	85	110	120
$\sigma_\infty^{TPV(chemEPDM)}$ [MPa]	0.75	0.76	0.77	0.79	0.81	0.836	0.87
$M_C^{TPV(chemEPDM)}$ [g/mol]	3833	3925	4013	4050	4067	4100	4088
$\sigma_\infty^{TPV(crystEPDM)}$ [MPa]	0.64	0.27	0.09	0	0	0	0
$M_C^{TPV(crystEPDM)}$ [g/mol]	4491	11,048	34,333	–	–	–	–
$\sigma_\infty^{TPV(crystPP)}$ [MPa]	0.6	0.48	0.45	0.26	0.12	0	0
$M_C^{TPV(crystPP)}$ [g/mol]	4791	6214	6866	12,305	27,452	–	–

totally. The decrease of the stress contribution $\sigma_\infty^{TPV(crystPP)}$ of the crystalline PP phase is explained by the change of the shape of the crystalline net points due to the ease of the slipping process when temperature increases.[8] When the crystalline PP phase starts to melt at $T_{m,onset}^{PP} = 105°C$, $\sigma_\infty^{TPV(crystPP)}$ reaches a value of zero. At this temperature the crystalline net points becomes too soft to keep the network stable. After $T_{m,onset}^{PP}$ the stress σ_∞^{TPV} is determined only by the contribution of the chemical network $\sigma_\infty^{TPV(chemEPDM)}$ of the EPDM phase. $\sigma_\infty^{TPV(chemEPDM)}$ increases with increasing temperature according to the entropy elasticity theory described by eq. (6).[21]

$$\sigma_\infty^{TPV(chemEPDM)} = (\lambda - \lambda^{-2}) E_\infty^{TPV(chemEPDM)} = (\lambda - \lambda^{-2}) \frac{3pkT}{M_C^{TPV(chemEPDM)}} \quad (6)$$

In eq. (6), the rubber elastic modulus $E_\infty^{TPV(chemEPDM)}$ is calculated from the non-relaxing stress component $\sigma_\infty^{TPV(chemEPDM)}$ and the draw ratio λ. It depends also on the density ρ, the Boltzmann constant k, the absolute temperature T and the average molecular weight between cross-links $M_C^{TPV(chemEPDM)}$.Using eq. (6) the apparent molecular weight $M_C^{TPV(crystEPDM)}$ and $M_C^{TPV(crystPP)}$ of the crystalline network of EPDM and PP phase, respectively, can be also determined. In Table IX, the molecular weight M_C of three networks is presented with increasing temperatures.

The calculated molecular weights M_C of three networks are depicted in Figure 6 as a function of test temperatures. Since the chemically cross-linked EPDM network is stable with time and temperature, the value of $M_C^{TPV(chemEPDM)}$ remains unchanged for the whole temperature range investigated. $M_C^{TPV(crystEPDM)}$ and $M_C^{TPV(crystPP)}$ increase to very high values due to the shape change of the crystalline net points induced by their melting processes.

The temperature dependence of the relaxing stress $\Delta\sigma^{TPV}$ shown in Figure 7 is described by two straight lines which intersect each other at $T_{m,end}^{EPDM} = 60°C$. As discussed in our previous works,[7,8,20] the decrease of $\Delta\sigma^{TPV}$ in the range between the room temperature and the melting temperature of PP is caused by the α-relaxation processes of the crystalline PP phase. The extrapolation of this straight line to zero intersects the x-axis at 160°C which corresponds to the melting point of the crystalline PP phase. The decrease of $\Delta\sigma^{TPV}$ in the temperature range between 30°C and 60°C is related to the α-relaxation processes inside the crystalline phase of ethylene segments of the EPDM phase. The segment-exchange of the molecules between the amorphous and crystalline phase at the interphase has been suggested as the nature of the

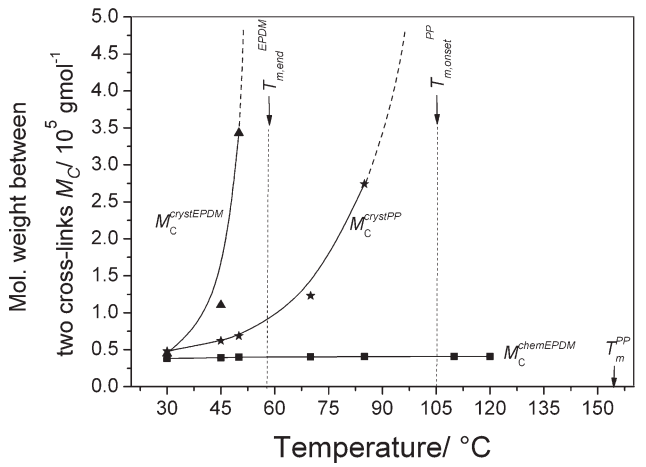

Figure 6 Temperature dependence of the molecular weight M_C of three networks.

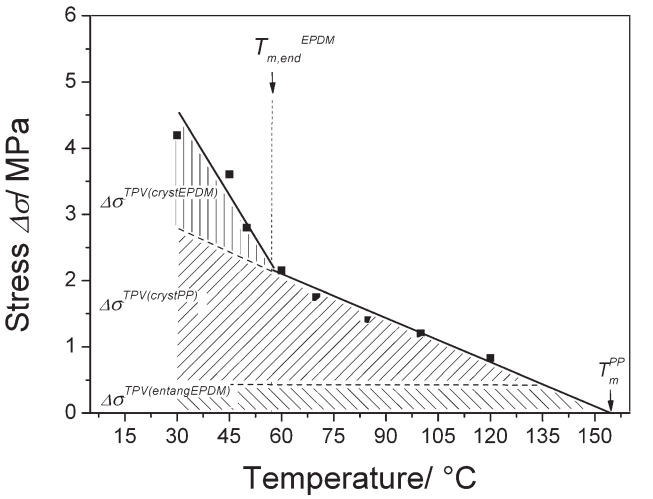

Figure 7 Relaxing stress $\Delta\sigma^{TPV}$ of TPV in dependence on the test temperatures.

α-relaxation processes in PP and PE.[22–25] The activation energy of the α-relaxation processes of ethylene segments determined in[22] is in the range from 115 kJ/mol to 140 kJ/mol depending on the segment length. The contribution of the α-relaxation processes of the PP and EPDM phase to $\Delta\sigma^{TPV}$ can be described by the relaxing stress $\Delta\sigma^{TPV(crystPP)}$ and $\Delta\sigma^{TPV(crystEPDM)}$. A unnegligible contribution of entanglements of EPDM phase, $\Delta\sigma^{TPV(entangEPDM)}$, to $\Delta\sigma^{TPV}$ can be seen in Figure 7. An exact determination of $\Delta\sigma^{TPV(entangEPDM)}$ has not been done in the present work. However, according to the previous work,[26] the value of $\Delta\sigma^{TPV(entangEPDM)}$ is about 40% of $\Delta\sigma^{TPV(chemEPDM)}$.

To describe the long-term behavior of TPV, a master curve was created by shifting the relaxation curves measured at different temperatures to a reference curve according to the superposition principle. However, in a thermo-rhelogically complex material like TPV a horizontal shift procedure can be done only for the relaxing stress curves $\Delta\sigma(t)$.[7,8,20,26] According to eq. (4), the relaxation curves $\sigma^{TPV}(t)$ of TPV measured at different temperatures were subtracted by the non-relaxing stress component σ_∞^{TPV} resulting in the relaxing stress curves $\Delta\sigma^{TPV}(t)$. The relaxing stress curves $\Delta\sigma^{TPV}(t)$ were horizontally shifted to a reference curve measured at 60°C. It is obvious that the curves measured at 30°C, 45°C and 50°C intersect each other and do not fit to the reference curve, whereas the curves measured at higher temperature were shifted well to that (Fig. 8). The reason for the failure of the formation of the master curve for temperatures below 60°C is the presence of the melting process of the crystalline EPDM phase which overlaps with the α-relaxation processes of PP.

To identify the physical background of the relaxing stress component the horizontal shift factor a_T was presented in dependence on the reciprocal temperature as shown in Figure 9. The temperature dependence of the horizontal shift factors a_T at temperatures between 60°C and 100°C follows the Arrhenius approach,[14] that means only one relaxation process takes place in this temperature range. From the slope of the straight line an activation energy of $E_A = 103$ kJ/mol was calculated. This activation energy is close to the activation energy of the α-relaxation process of the crystalline PP phase measured in this temperature range determined in our previous work ($E_A = 110$ kJ/mol)[7,8] for PP/NBR blends and to the corresponding results in the literature (107–150 kJ/mol) for PP.[27] At the test temperatures above $T_{m,\text{onset}}^{PP}$ the crystalline PP phase becomes softening and as a result a low activation energy of 50 kJ/mol for the α-relaxation process was found.

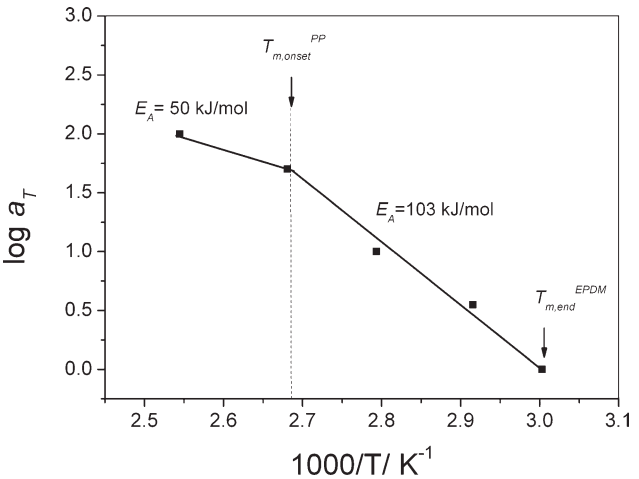

Figure 9 Temperature dependence of the horizontal shift factor log a_T.

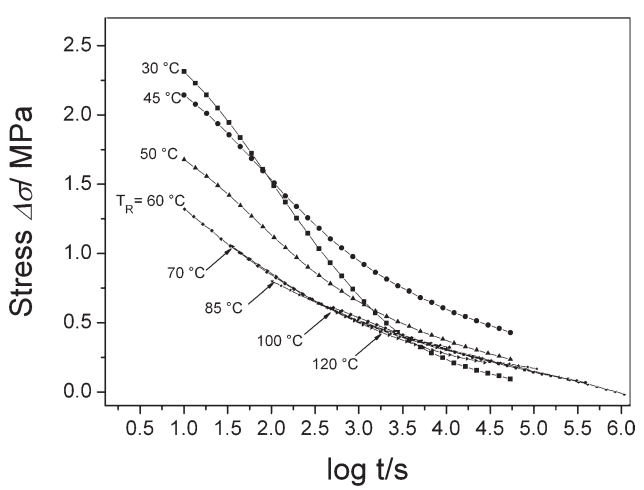

Figure 8 Master curve created by the horizontal shift of the relaxing stress curves $\Delta\sigma^{TPV}(t)$ of TPV to the reference curve measured at 60°C.

Stress relaxation of filled TPV

Owing to the reinforcement effect of CB, the stress relaxation behavior of composites is influenced strongly by CB addition. To facilitate the discussion of the background of the stress components induced by CB addition, the formation of CB network and structure of the polymer-layer bound to the CB surface should be taken into account. In a CB filled polymer compound, the existence of a polymer-layer adsorbed on the CB surface is generally accepted. Such polymer-layer can be visualized in Figure 10(a) which shows a TEM image of a polymer-filler gel made by Ono et al.[28] It is clear to observe a polymer-layer surrounding the filler aggregates after extraction experiments. The average thickness of this layer is approximately 20.0 nm. According to the two-phase shell structure[29,30] the polymer-layer consists of two components, a relatively mobile

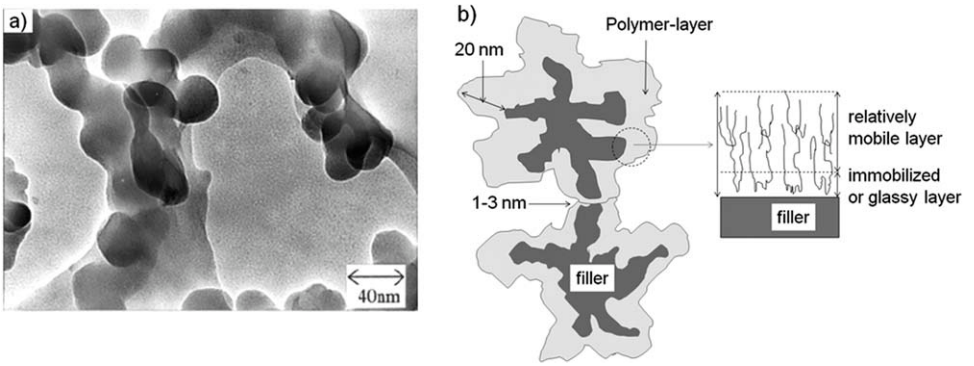

Figure 10 TEM image of a rubber-filler gel[28] (a) and scheme of CB network and polymer-layer bound to the CB surface (b).

component and an immobilized one as schematically illustrated in Figure 10(b). A literature study pointed out that the thickness of the immobilized layer actually depends on the polymer-filler interaction and on the method which is used to probe it.[31] According to the nuclear magnetic resonance (NMR) investigations on CB filled EPDM compounds made by Kaufman,[30] in close vicinity to the CB surface within 1 nm there is a thin layer of polymer whose mobility is extremely restricted due to the interaction with the CB surface. Donth and coworkers.[32] using rheological data, estimated the thickness of the immobilized layer in SBR to be 1.5 nm. Arrighi et al.[33] found a layer thickness of 5.0 nm for silica-filled poly(dimethylsiloxane), whereas Litvinov and Spiess[34] estimated 0.8 nm for this system using ^{2}H-NMR as the probe. This immobilized layer is characterized by a glass temperature $T_G^{\text{immobilized}-\text{layer}}$, exceeding it the immobilized layer becomes mobile. A $T_G^{\text{immobilized}-\text{layer}}$ of 10°C for SBR-silica composites was found by Arrighi et al.[35] by means of dynamic mechanical analysis. Using NMR technique for CB filled EPDM compounds Kaufman[30] found that $T_G^{\text{immobilized}-\text{layer}}$ decreases from the outer boundary of the polymer-layer towards the CB surface that indicates the thickness of the immobilized layer decreases with increasing temperature. The immobilized layer of 1.0 nm thickness closed to the CB surface has a $T_G^{\text{immobilized}-\text{layer}}$ of about 100°C.

As observed in Figure 10(a,b), filler aggregates are connected together by a thin polymer-layer forming a throughout network. Because a conductive CB network is formed in the investigated composites excepting the C-9CB1-E, electrons can then jump cross the gap between two aggregates according to the hopping model. Using 3D-TEM technique Kohjiya et al.[36] calculated that the gap in a conductive network lies in an order of about 1.0–3.0 nm. In such narrow gap, the thin polymer-layer exists in a glassy state.

The relaxation curves of composite C-9CB1-E lie in a higher level in comparison to those of TPV as shown in Figure 11. With increasing temperatures the relaxation curves also shift vertically to lower level and horizontally to shorter time. Interestingly, the curve of the composite measured at 120°C has the same level like that of TPV shown in Figure 4. CB addition seems not to have effect on the relaxation behavior at these temperatures. The reason will be investigated in details later.

Based on an assumption that all the networks available in the composite are combined in a parallel circuit,[37] the non-relaxing and relaxing stress component σ_∞^{CB} and $\Delta\sigma^{CB}$, respectively, which are induced by CB addition can be determined by σ_∞^{Comp} and $\Delta\sigma^{Comp}$ of the composite, and σ_∞^{TPV} and $\Delta\sigma^{TPV}$ of the composite matrix with regard to the volume concentration φ^{CB} of CB according to the eqs. (7) and (8).

$$\sigma_\infty^{CB} = \sigma_\infty^{comp} - (1 - \varphi^{CB})\sigma_\infty^{TPV} \tag{7}$$

and

$$\Delta\sigma^{CB} = \Delta\sigma^{comp} - (1 - \varphi^{CB})\Delta\sigma^{TPV} \tag{8}$$

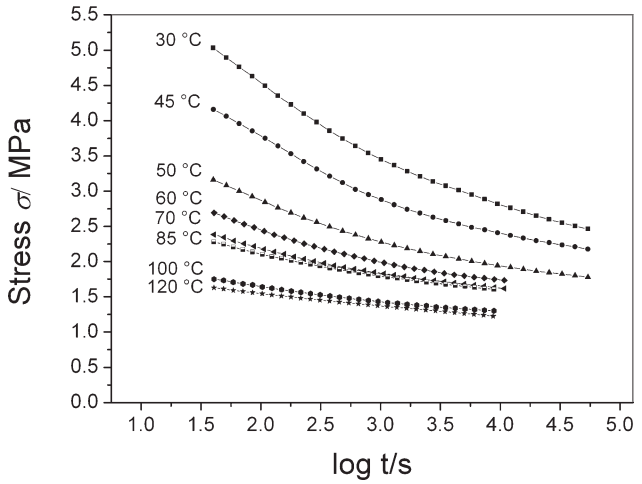

Figure 11 Relaxation curves of C-9CB1-E in dependence on test temperatures.

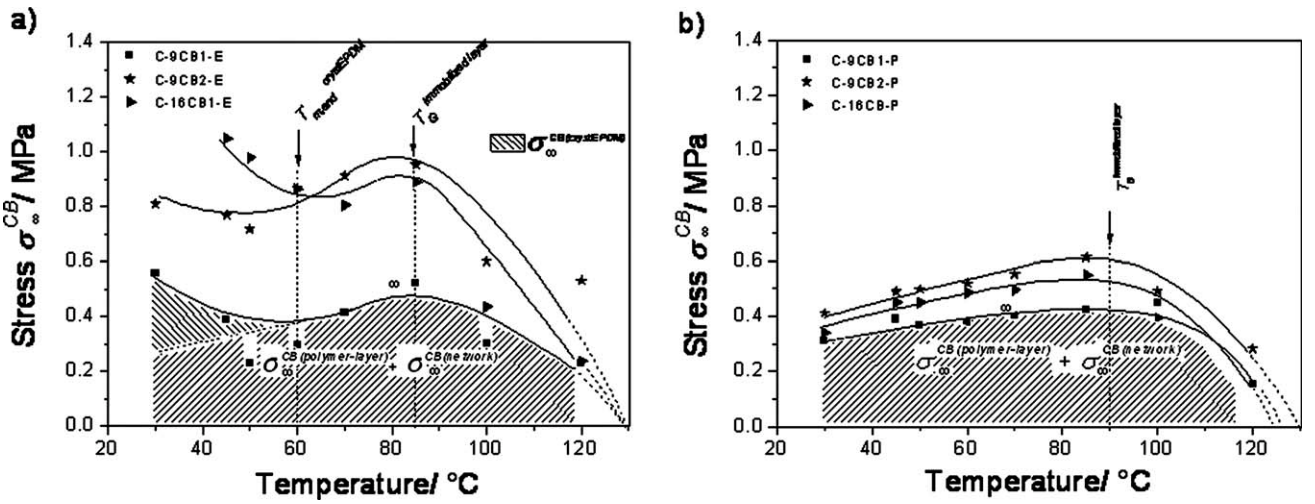

Figure 12 Non-relaxing stress σ_∞^{CB} of different composites with CB localization in EPDM phase, series E (a) and PP phase, series P (b).

The non-relaxing stress σ_∞^{CB} of different composites with CB localization in the EPDM phase and PP phase is presented in Figure 12(a,b), respectively, in dependence on test temperatures. The non-relaxing stress σ_∞^{CB} induced by CB addition can be generally divided into the stress component $\sigma_\infty^{CB(polymer-layer)}$ and $\sigma_\infty^{CB(network)}$.[26] $\sigma_\infty^{CB(polymer-layer)}$ is the non-relaxing stress components resulted from the time stable polymer-CB bonds which are available in the polymer-layer bound on the CB surface. According to the work of Maier and Göritz[38] a distribution of differently strong links between filler particles and segments of elastomer chains exists. During mixing, the first macromolecules that come in contact with the filler "see" the whole free surface. When a first link is formed, neighboring segments have a higher probability to attach to the next interaction position and so on. This process comes to an end when all neighboring sites on the filler surface are occupied. Chains, which arrive at the surface at a later moment, find the area widely covered and their possibilities of stabilization are reduced. The last chains attached to the sites have very week links to the particle.

$\sigma_\infty^{CB(network)}$ is originated by the stable CB network fraction whose gaps between CB aggregates are smaller than approximately 3.0 nm. The glassy thin polymer-layer in these gaps can keep the CB network stable against the impact of applied stresses. According to the morphological investigations and electrical resistivity measurement, in C-9CB1-E, CB1 does not form any network, thus, the stress component $\sigma_\infty^{CB(network)}$ does not exist in C-9CB1-E.

In both series E and P, σ_∞^{CB} increases with increasing temperatures up to 90°C that results from the entropy elastic forces. Comparing to $\sigma_\infty^{TPV(chemEPDM)}$ of the unfilled TPV (Fig. 5), σ_∞^{CB} increases more strongly, because it is originated from a higher cross-link density contributed by chemical net points, polymer-CB bonds and filler-filler bonds.

It is interesting to observe that at temperatures higher than 90°C σ_∞^{CB} decreases strongly in both series. One reason is related to the softening of the thin polymer layers connecting two CB aggregates when the test temperature exceeds the $T_G^{immobilized-layer}$. The thin polymer layer leaves its glassy state and becomes softened that makes the CB network looser and more instable against the mechanical impact. In such state, the elastic stress induced by the CB network decays rapidly. In this work, a $T_G^{immobilized-layer}$ of about 90°C detected in both series is according to that reported by Kaufman.[30] Thus, the contribution of $\sigma_\infty^{CB(network)}$ diminishes with increasing temperature. Although a CB network does not exist in the composite C-9CB1-E, $\sigma_\infty^{CB(polymer-layer)}$ decays also rapidly after 90°C. That indicates that softening of the immobilized layer likely reduces the number of the stable polymer-CB bonds as well. Extrapolating σ_∞^{CB} to 0 intersects the x-axis at 130°C. At this temperature CB shows no reinforcement effect any more. That is why the relaxation curve of composites measured at 120 °C as shown in Figure 11 lies nearly in a level of that of TPV as shown in Figure 4.

The decrease of σ_∞^{CB} in the temperature range up to 60°C is observed only in the series E when CB localizes in the EPDM phase as presented in Figure 12(a). That is attributed to the melting of the crystalline EPDM phase. Although the investigation of the crystalline phases using DSC shows only small effect of CB addition (Table VII), the results by means of wide angle X-ray scattering measurements (WAXS) reported in different works[39–41] emphasize the significant nucleating effect of CB on the structure of the crystalline phase. Thus, the presence of CB in EPDM phase likely modifies the EPDM crystalline

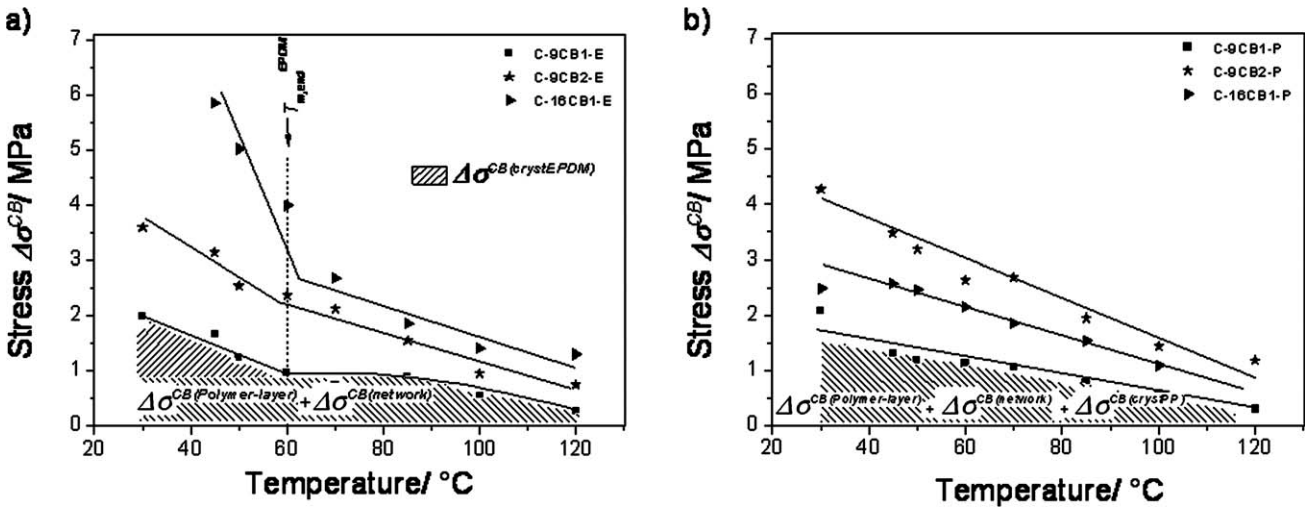

Figure 13 Relaxing stress $\Delta\sigma^{CB}$ of different composites with CB localization in the EPDM phase (a) and PP phase (b).

phase and causes an additional contribution $\sigma_{\infty}^{CB(crystEPDM)}$.

Addition of a higher concentration CB1 in TPV (C-16CB1-E) shifts σ_{∞}^{CB} upwards a high level as shown in Figure 12. The main reason is a formation of a CB network causing a high value of $\sigma_{\infty}^{CB(network)}$. CB2 has a large specific surface area causing a high value of EPDM-layer, and at the same time it also forms a CB network. The high level of σ_{∞}^{CB} by addition of CB2 is resulted from the high values of $\sigma_{\infty}^{CB(polymer-layer)}$ and $\sigma_{\infty}^{CB(network)}$.

The impact of CB on the σ_{∞}^{CB} is more pronounced in series E than series P. That is related to the fact that in TPV the PP matrix controls the mechanical behavior in the small deformation scale, and in the large deformation scale, for instance at a draw ratio $\lambda = 2.0$ as seen in the present work, the EPDM phase dominantly determines the mechanical behavior.

The relaxing stress component $\Delta\sigma^{CB}$ of the series E was calculated using eq. (8) and presented in Figure 13(a). It decreases with increasing test temperature. In the temperature range above 60°C, the relaxing stress $\Delta\sigma^{CB}$ is the sum of $\Delta\sigma^{CB(polymer-layer)}$ and $\Delta\sigma^{CB(network)}$. $\Delta\sigma^{CB(polymer-layer)}$ is originated from the *debonding* processes taking place inside the polymer-layer surrounding CB aggregates. The *debonding* process was computerized in different works[42,43] using finite element methods. Using the unit cell model containing four spherical CB particles, Matouš and Geubelle[44] revealed that the debonding is first detected at the pole of a particle due to the stress concentration. The debonding of particle leads to the unloading of this matrix region,

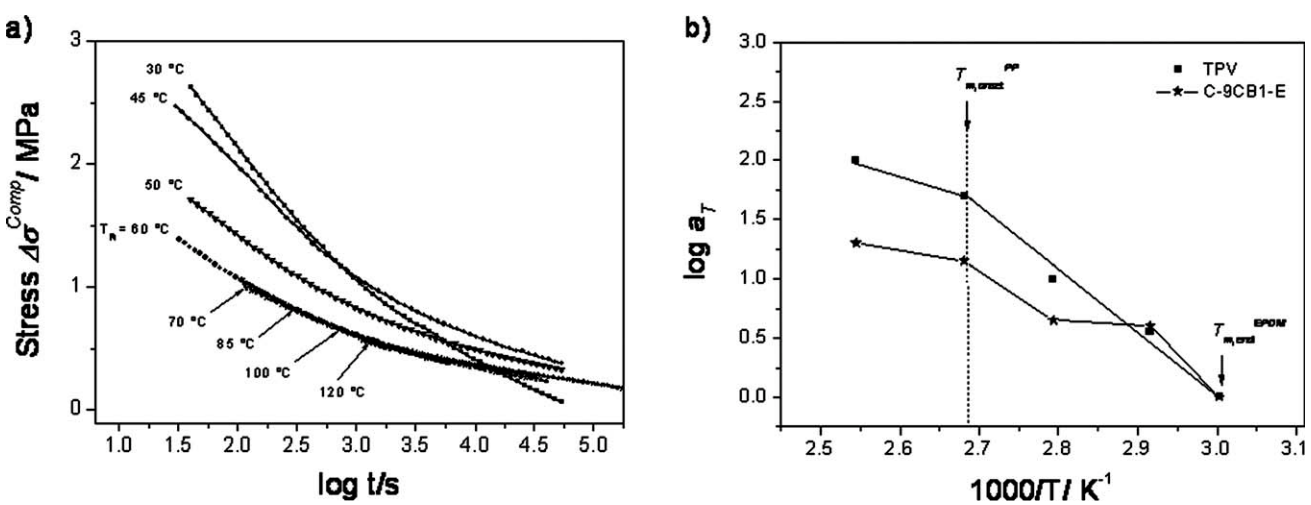

Figure 14 Master curve created by the horizontal shift of the relaxing stress curves $\Delta\sigma^{Comp}(t)$ of the composite C-9CB1-E to the reference curve at 60°C (a), and the temperature dependence of the horizontal shift factor a_T (b).

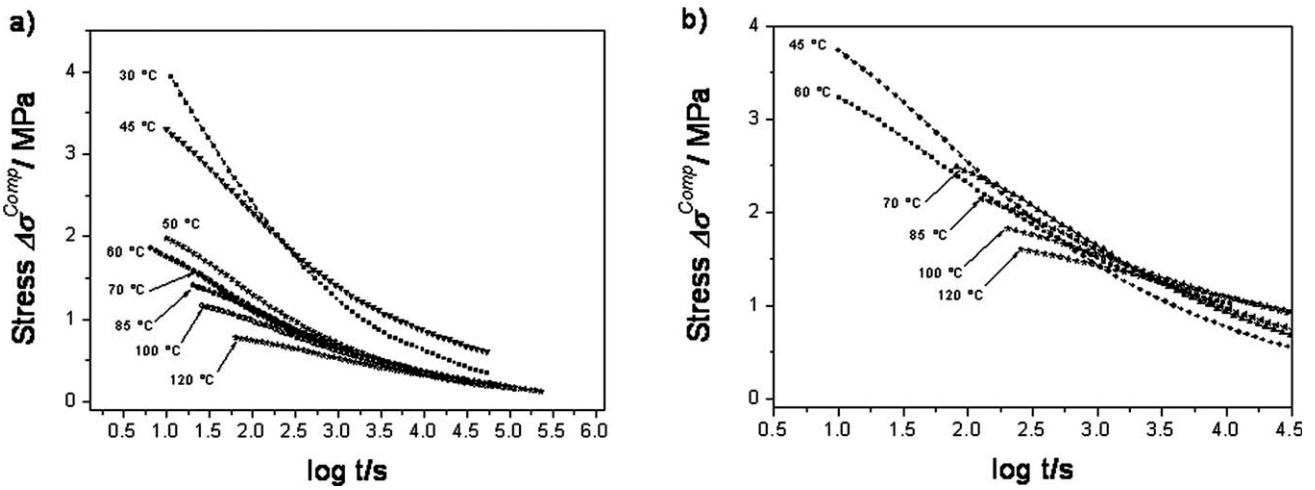

Figure 15 Master curves created by the horizontal shift of the relaxing stress curves $\Delta\sigma^{Comp}(t)$ of the composite C-9CB1-P (a) and C-16CB1-E (b) to the reference curve at 60°C.

and the next debonding is generated in the vicinity of the nearest particle. These debonding events take place in a relatively progressive fashion. Lu and Tomita.[43] also used the cohesive zone model to describe the process of debonding around carbon black. At a critical stress-state, void nucleation occurs inside the relatively mobile polymer layer and leads to the onset of debonding around carbon black, which is important to the deformation resistance, hysteresis loss and the volume dilatation of carbon black filled rubber. The work also clarified the effects of critical interfacial strength and the characteristic length, and volume fraction of carbon black as well as heterogeneity of the density of molecular chains around carbon black on the debonding processes. It was proved experimentally that in the absence of a good interfacial bond, fillers will pull out of the polymer and result in an annulment of the reinforcing effect.[45] Controlled *debonding* at the weak polymer-filler interface, on the other hand, results in increased toughness of the system, but at the cost of concurrent decrease in the transverse strength on fatigue resistance.[46] The toughness of a filled polymer material can be adjudged by the behavior of the polymer-filler interface during fracture. However, the presence of an immobilized/glassy polymer layer close to the CB surface was not taken into consideration in those discussions. It is likely impossible for the glassy polymer shell to debond itself from the CB surface. The $\Delta\sigma^{CB(polymer\text{-}layer)}$ is supposed to be related to the *debonding* process of the relatively mobile chains closed to the glassy immobilized layer.

$\Delta\sigma^{CB(network)}$ is caused by the temperature induced collapse of the CB network fraction whose gaps between two aggregates larger than 3.0 nm The thin polymer-layer available in these wide gaps can be softening at temperatures lower than $T_G^{immobilized-layer}$. Vennemann and coworkers[47] suggested that an increase in temperature would further aid in weakening filler-filler bonds. According to our previous work[26] up to 70°C the relaxing stress $\Delta\sigma^{CB(polymer\text{-}layer)}$ dominates and at temperatures higher than 70°C the collapse of the bending-twisting deformed filler-filler bonds is supposed as a new relaxation process. In the temperature range up to 60°C, an additional stress component $\Delta\sigma^{CB(crystEPDM)}$ is detected for series E but not for series P. It is related to the α-relaxation process of the crystalline EPDM phase which is additionally influenced in presence of CB.[41]

In Figure 13(b), the relaxing stress $\Delta\sigma^{CB}$ consisting of $\Delta\sigma^{CB(polymer\text{-}layer)}$, $\Delta\sigma^{CB(network)}$ and $\Delta\sigma^{CB(crystPP)}$ decreases strongly with temperature. The $\Delta\sigma^{CB(network)}$ is caused by the collapse of the CB network in the PP phase. The α-relaxation process of the crystalline PP phase contributes to the $\Delta\sigma^{CB(crystPP)}$ and the *debonding* process of PP molecules from the CB surface to the $\Delta\sigma^{CB(polymer\text{-}layer)}$.

The master curve created by horizontal shift of the relaxing stress curves $\Delta\sigma^{Comp}(t)$ of the composites C-9CB1-E to the curve measured at reference temperature $T_R = 60°C$ is presented in Figure 14(a). Only the curves measured at temperatures higher than 60°C fit very well to the reference curve. As discussed above, there are different processes taking place in this temperature range but compared to the α-relaxation process of the crystalline PP phase, the *debonding* process and the collapse of the CB network in this composite are considered as negligible. Thus, the master curve describes the α-relaxation process as the main relaxation process in this temperature range. The temperature dependence of the horizontal shift factor a_T of the composites C-9CB1-E is presented in comparison with that of TPV [Fig. 14(b)].

It consists of different straight lines meaning different stress relaxation processes in this temperature range.

When the formation of the polymer-layer and CB network increases to a larger extent, the impact of the *debonding* process and the collapse of the CB network on the stress relaxation becomes innegligible. It is now impossible to create a master curve as seen in Figure 15(a) for C-9CB1-P and in Figure 15(b) for C-16CB1-E.

CONCLUSIONS

Discussion of the effect of CB on the stress relaxation of CB filled TPV is focused on the stress components which are originated from the CB addition, the non-relaxing stress components $\sigma_{\infty}^{CB(polymer-layer)}$ and $\sigma_{\infty}^{CB(network)}$, as well as the relaxing stress components $\Delta\sigma^{CB(polymer\text{-}layer)}$ and $\Delta\sigma^{CB(network)}$. $\sigma_{\infty}^{CB(polymer-layer)}$ is determined by the number of the stable polymer-CB bonds, whereas $\Delta\sigma^{CB(polymer\text{-}layer)}$ is characterized by the *debonding* processes of the polymer chains from the CB surface. $\sigma_{\infty}^{CB(network)}$ is caused by the stable CB network factions, and $\Delta\sigma^{CB(network)}$ is originated by the collapse of the instable CB network fractions. It was found that the concentration and type of CB as well as the phase specific CB distribution strongly affect the non-relaxing and relaxing stress components. A glass temperature of the immobilized polymer layer of about 90°C was detected, exceeding it the glassy thin polymer-layers which connect CB aggregates together forming a network are softened, and the effect of CB on the stress relaxation behavior diminishes. A master curve was created by horizontal shift of the relaxing stress curves $\Delta\sigma^{Comp}(t)$ to a reference curve for TPV filled with 9% CB in the EPDM phase. At this concentration filled TPV still remains as a thermo-rheologically simple material, because the impact of CB addition on the stress relaxation of TPV is still negligible. At higher local CB loadings, the additional relaxation processes induced by CB addition overlap with the α-relaxation process of the crystalline PP phase. Thus, no master curve could be made.

References

1. Coran, A. Y.; Patel, R. P. Rubber Chem Technol 1980, 5, 141.
2. Xiao, H. W.; Huang, S. Q.; Jiang, T. J Appl Polym Sci 2004, 92, 357.
3. Babu, R. R.; Singha, N. K.; Naskar, K. Express Polym Lett 2008, 2, 226.
4. Le, H. H.; Tiwari, M.; Ilisch, S.; Radusch, H.-J. Plast Rubber Compos 2006, 35, 410.
5. Katbab, A. A.; Nazockdast, H.; Bazgir, S. J Appl Polym Sci 2000, 75, 1127.
6. Katbab, A. A.; Hrymak, A. N.; Kasmadjian, K. J Appl Polym Sci 2007, 107, 3425.
7. Le, H. H.; Lüpke, T.; Pham, T.; Radusch, H.-J. Polymer 2003, 40, 4589.
8. Le, H. H.; Zia, Q.; Ilisch, S.; Radusch, H.-J. Expr Polym Lett 2008, 2, 791.
9. Long D.; Sotta, P. Rheol Acta 2007, 46, 1029.
10. Baeurle, S. A.; Hotta, A.; Gusev, A. A. Polymer 2005, 46, 4344.
11. Asaletha, R.; Bindu, P.; Aravind, I.; Meera, A. P.; Valsaraj, S. V.; Yang, W.; Thomas, S. J Appl Polym Sci 2008, 198, 904.
12. Seeger, A. Handbuch Der Physik; Springer: Berlin, 1958.
13. Seeger, A. Z. Naturforsch 1954, 9a, 758.
14. Krausz, A. S.; Eyring, H. Deformation Kinetics; Wiley: New York, 1975.
15. Ferry, J. D. Viscoelastic Properties of Polymers; Wiley: New York, 1980.
16. Wunderlich, B.; Czornyj, G. Macromolecules 1977, 10, 906.
17. Xenopoulos, A.; Wunderlich, B. J Polym Sci: Polym Phys Ed 1990, 28, 2271.
18. Li, J. C. M. Can J Phys 1967, 45, 493.
19. Koszkul, J. Mater Sci 1999, 35, 81.
20. Le, H. H. Ph.D. Thesis, Martin Luther University, Halle-Wittenberg, Germany, 2002.
21. Treloar, L. R. G. The Physics of Rubber Elasticity; Clarendon Press: Oxford, 1975.
22. Kolesov, I. S.; Androsch, R.; Radusch, H.-J. Macromolecules 2005, 38, 445.
23. Boyd, R. H. Polymer 1985, 26, 1123.
24. Buckley, C. P.; McCrum, N. G. J Mater Sci 1973, 8, 928.
25. Boyd, R. H. Polymer 1985, 26, 323.
26. Le, H. H.; Ilisch, S.; Radusch, H.-J. Polymer 2009, 50, 2294.
27. Brandrup, J.; Immergut, E. H. Polymer Handbook, 3rd ed.; Wiley: New York, 1989; p V/29.
28. Ono, S.; Kiuchi, Y.; Sawanobori, J.; Ito, M. Polym Int 1999, 48, 1035.
29. Kraus, G.; Rollmann, K. W.; Gruver, J. T. Macromolecules 1970, 3, 92.
30. Kaufman, S. J Polym Sci Part A-2: Polym Phys 1971, 9, 829.
31. Ozmusul, M. S.; Picu, R. C. Polymer 2002, 43, 4657.
32. Vieweg, S.; Unger, R.; Hempel, E.; Donth, E. J Non-Cryst Solids 1998, 35, 337.
33. Arrighi, V.; Higgins, J. S.; Burgess, A. N.; Floudas, G. Polymer 1998, 39, 6369.
34. Litvinov, V. M.; Spiess, H. W. Makromol Chem 1991, 192, 3005.
35. Arrighi, V.; McEwen, I. J.; Qian, H.; Serrano Prieto, M. B. Polymer 2003, 44, 6259.
36. Kohjiya, S.; Katoh, A.; Suda, T.; Shimanuki, J.; Ikeda, Y. Polymer 2006, 47, 3298.
37. Isono, Y.; Ferry, J. D. Rubber Chem Technol 1984, 57, 925.
38. Maier, P. G.; Göritz, D. Kautsch Gummi Kunsts 1990, 49, 18.
39. Petrovic, Z. S.; Martinovic, B.; Divjakovic, V.; Budinski-Simendic, J. J Appl Polym Sci 2003, 49, 1659.
40. Omastová, M.; Prokes, J.; Kosina, S.; Hlavatá, D. Macromol Symp 2001, 170, 241.
41. Rieker, T. P.; Hindermann-Bischoff, M.; Ehrburger-Dolle, F. Langmuir 2000, 16, 5588.
42. Matouš, K.; Geubelle, P. H. Int J Numer Methods Eng 2006, 65, 190.
43. Lu, W.; Tomita, Y. WCCM VI in Conjunction with APCOM'04, Beijing, China, September 5–10, 2004.
44. Matouš, K.; Geubelle, P. H. Int J Numer Methods Eng 2006, 65, 190.
45. Cessna, L. C.; Thomson, J. B.; Hanna, R. D. SPE J 1969, 25, 35.
46. Cook, J.; Gordon, J. Proc R Soc 1964, 4282, 508.
47. Srinivasan, N.; Bökamp, K.; Vennemann, N. Kautsch Gummi Kunstst 2005, 58, 650.